



Nuclear corrections on the charged hadron fragmentation functions in a Neural Network global QCD analysis

Maryam Soleymaninia¹ ^{*}, Hadi Hashamipour^{1,†}, Hamzeh Khanpour^{2,3,4,1} [‡], Samira Shoeibi^{1,§}, and Alireza Mohamaditabar^{1,¶}

¹*School of Particles and Accelerators, Institute for Research in Fundamental Sciences (IPM), P.O.Box 19395-5531, Tehran, Iran*

²*Dipartimento Politecnico di Ingegneria ed Architettura, University of Udine, Via della Scienze 206, 33100 Udine, Italy.*

³*International Centre for Theoretical Physics (ICTP), Strada Costiera 11, 34151 Trieste, Italy.*

⁴*Department of Physics, University of Science and Technology of Mazandaran, P.O.Box 48518-78195, Behshahr, Iran*

(Dated: May 5, 2023)

In this work, we present the new global QCD analyses, referred to as PKHFF.23, for charged pion, kaon, and unidentified light hadrons by utilizing the Neural Network for fitting the high energy lepton-lepton and lepton-hadron scattering to determine parton-to-hadron fragmentation functions (FFs) at both next-to-leading-order (NLO) and next-to-next-to-leading-order (NNLO) accuracy. The analyses include all available single-inclusive e^+e^- annihilation (SIA) and semi-inclusive deep-inelastic scattering (SIDIS) data for charged pions, kaons, and unidentified light hadrons. Considering the most recent nuclear parton distribution functions (nuclear PDFs) available in the literature, we assess the impact of nuclear corrections on the determination of light hadrons FFs. We show that considering the nuclear corrections at both NLO and NNLO accuracy affect the central values of FFs and the associated uncertainty bands, and could improve the fit quality as well. The Neural Network parametrization enriched with the Monte Carlo methodology for uncertainty estimations is used for all sources of experimental uncertainties and the proton PDFs.

CONTENTS

I. Introduction	1
II. Theoretical Setup	2
III. Experimental Data Setup	3
IV. Analysis setup and fitting procedure	3
V. Numerical Results	4
A. Nuclear effects of the kaon FFs	4
B. Nuclear effects of the unidentified light charged hadron FFs	5
C. Nuclear effects of the pion FFs	7
VI. Summary and Conclusions	8
Acknowledgments	9
References	18

I. INTRODUCTION

Fragmentation Functions (FFs) play an important role to study the non perturbative parton structure of

hadrons at the Large Hadron Collider (LHC), and future high-precision hadron production measurements at Electron Ion Collider (EIC) [1, 2] and Future Circular Collider (FCC) [3, 4]. Hence, up-to-date methodological, experimental and theoretical developments need to be considered to calculate well-established FF sets as well. To this end, most recently, several global QCD analyses have been performed to determine the FFs of charged pion and kaon [5], and unidentified light hadrons [6] by including all available data from single inclusive electron-positron annihilation (SIA) and semi-inclusive deep-inelastic scattering (SIDIS) processes. The Neural Network (NN) as a modern optimization technique to minimize the bias of parametrization is considered. In order to obtain the probability density distribution in the fitting analysis, the Monte Carlo method has been employed. These analyses have been performed using the publicly available **MontBlanc** package [7]. The analysis for FFs of unidentified light charged hadrons has been extracted up to next-to-leading order (NLO), and the FFs of pion and kaon have been determined up to next-to-next-to-leading order (NNLO) accuracy.

The perturbative corrections for SIA up to NNLO are available [8, 9], and recently the derivation of approximate NNLO corrections to SIDIS has been completed by expanding the resummed expressions [10]. The authors of Ref. [5] have extended the theoretical accuracy up to NNLO corrections as well. Consequently, the **MontBlanc** package takes advantages of these developments and could calculate the FFs for different hadrons up to NNLO by including SIA and SIDIS measurements.

Although the recently reported FF sets [5, 6] take advantage of the model bias reduction in FF parametriza-

* Maryam_Soleymaninia@ipm.ir

† H_Hashamipour@ipm.ir

‡ Hamzeh.Khanpour@cern.ch

§ Samira.Shoeibi@ipm.ir

¶ A.Mohamaditabar@ipm.ir@ipm.ir

tion, in the propagation of the experimental data and in the proton PDFs uncertainties, the nuclear corrections have not been taken into account so far. The cross section in the SIDIS process is calculated considering only the proton PDFs set at NLO and NNLO accuracy and the analyses have been performed without considering the nuclear corrections on the PDFs in SIDIS.

In this work, we mainly focus on the revisiting the analyses mentioned above for charged (π^\pm), kaon (K^\pm) and unidentified light hadrons (H^\pm) in order to consider the impact of various nuclear PDF sets in determination of FFs. To this end, we first perform the global QCD analyses for FFs of charged pion, kaon and unidentified light hadrons separately by considering the **NNPDF3.1** [11] proton PDF set as a baseline fit in the case of SIDIS for both NLO and NNLO accuracy. Then we repeat the analyses considering the most recent nuclear PDF sets to investigate the effects of applying the nuclear corrections. We produce three FF sets by utilizing **nNNPDF3.0** [12], **EPS21** [13] and **nCTEQ15WZ** [14] nuclear PDF sets at NLO, and one FF set by utilizing **nNNPDF1.0** [15] nuclear PDF sets at NNLO accuracy. We study the impact of nuclear corrections in determination of FFs in the global NLO and NNLO QCD analyses, and the main results and findings are clearly presented and discussed. We show that the nuclear corrections could affect both the shape and uncertainty bands, and could improve the fit quality as well.

The rest of the paper is organized as follows. In Sec. II we summarize the theoretical formalism for the SIA and SIDIS processes. The parametrization of FFs and the flavor decomposition for charged pion, kaon and unidentified light hadrons in terms of Neural Network will be detailed in this section. The SIA and SIDIS experimental data sets analyzed in this work and the kinematical cuts applied will be summarized in Sec. III. In Sec. IV we present the fitting methodology as well as the Monte Carlo method to calculate the uncertainties of FFs. Sec. V includes the detailed discussion of the numerical results in the presence of nuclear corrections. Finally, Sec. VI present the summary and conclusion.

II. THEORETICAL SETUP

According to the standard collinear factorization, the QCD cross sections can be separated into the perturbative partonic cross sections convoluted with the partonic and hadronic distribution functions as non-perturbative objects [16]. Therefore, the cross sections for SIA and SIDIS can be written as,

$$\begin{aligned}\sigma^{\text{SIA}} &= \hat{\sigma} \otimes \text{FF}, \\ \sigma^{\text{SIDIS}} &= \hat{\sigma} \otimes \text{PDF} \otimes \text{FF}.\end{aligned}\quad (1)$$

The $\hat{\sigma}$ indicates partonic cross section as a process dependent and perturbative part of the cross sections. The

universal and non-perturbative parts of the cross sections are indicated by PDFs and FFs. The details of the computation of the SIA and SIDIS cross sections can be found in the literature, and we refer the reader to Refs. [6, 17, 18] for a clear review.

The NLO and NNLO corrections to the time-like DGLAP evolution equations and to the SIA coefficient functions carried out in the literature [19, 20]. The NNLO corrections to SIDIS coefficient functions are taken from Ref. [10] in which the authors have calculated the NNLO perturbative corrections by applying the threshold resummation formalism up to next-to-next-to-leading logarithmic (NNLL) order. Then the approximate NNLO corrections to unpolarized and polarized SIDIS are achievable. Accordingly, in the present paper, we investigate the impact of nuclear correction on the FFs of charged hadrons at NLO and NNLO accuracy.

In the following we present the parameterization and flavor decomposition for charged pion, kaon and light hadrons at the initial scale $\mu_0 = 5$ GeV. Since the SIA data along with SIDIS measurements are included in our analyses, the direct constrain on the FFs of light quarks and antiquarks could be provided. In the case of pions and kaons, we follow the flavor decomposition of Ref. [5]

$$\begin{aligned}D_g^{\pi^+}, & & D_g^{K^+}, \\ D_u^{\pi^+}, & & D_u^{K^+}, \\ D_d^{\pi^+}, & & D_s^{K^+}, \\ D_d^{\pi^+} = D_{\bar{u}}^{\pi^+}, & & D_s^{K^+} = D_{\bar{u}}^{K^+}, \\ D_s^{\pi^+} = D_{\bar{s}}^{\pi^+}, & & D_d^{K^+} = D_{\bar{d}}^{K^+}, \\ D_c^{\pi^+} = D_{\bar{c}}^{\pi^+}, & & D_c^{K^+} = D_{\bar{c}}^{K^+}, \\ D_b^{\pi^+} = D_{\bar{b}}^{\pi^+}, & & D_b^{K^+} = D_{\bar{b}}^{K^+}.\end{aligned}\quad (2)$$

In the case of unidentified light charged hadrons, we follow the flavor decomposition as our previous work [6],

$$\begin{aligned}D_g^{H^+}, \\ D_u^{H^+}, \\ D_{\bar{u}}^{H^+}, \\ D_d^{H^+} = D_s^{H^+}, \\ D_{\bar{d}}^{H^+} = D_{\bar{s}}^{H^+}, \\ D_c^{H^+} = D_{\bar{c}}^{H^+}, \\ D_b^{H^+} = D_{\bar{b}}^{H^+}.\end{aligned}\quad (3)$$

These FFs are obtained in the framework of Neural Networks. Corresponding to the momentum fraction z , we use one input node in a one-layered feed-forward Neural Network, 20 intermediate nodes in a one hidden layer and a sigmoid activation function. Since the number of independent FFs of the positive pion, kaon and unidentified light hadrons are seven, we use 7 nodes in the

output with a linear activation function. The architecture of the Neural Network is $1 - 20 - 7$ and the number of Monte Carlo replicas is 200. Indeed, the uncertainty propagation has been estimated by using the Monte Carlo method.

As we mentioned before, the main aim in this paper is to investigate the impact of applying the nuclear corrections to calculate the SIDIS observables. To this end, in the first step, we use the proton PDF sets NNPDF3.1 [11] as input to calculate the SIDIS cross sections.

In the second step, the nuclear PDF sets are taken into account for the nuclear corrections. The computation of FFs at NLO accuracy has been performed by means of various nuclear PDF sets, namely the nNNPDF3.0 [12], EPPS21 [13] and nCTEQ15WZ [14] at NLO accuracy. For the NNLO accuracy we use nNNPDF1.0 nuclear PDF sets [15].

We determine the charged pion, kaon and light hadron FFs in the Zero-Mass Variable-Flavor-Number Scheme (ZM-VFNS), in which the active flavors are considered to be massless. In our analysis, the masses of charm and bottom quarks are considered to be fixed at $m_c = 1.51$ GeV and $m_b = 4.92$ GeV, respectively. Finally, we should mention that we utilize the `MontBlanc` public package for our global QCD analyses in this project.

III. EXPERIMENTAL DATA SETUP

The experimental data sets used in this work include both the SIA and SIDIS measurements for charged pion, kaon and unidentified light hadrons productions.

In the case of SIA, the measured differential cross section is normalized to the total cross section and reported as sum of the production of positively and negatively charged hadrons. The data analyzed in this work include different experiments performed by TASSO [21–24] experiment at DESY, TPC [25], BABAR [26] and SLD [27] experiment at SLAC, BELLE [28] and TOPAZ [29] at KEK, and ALEPH [30, 31], DELPHI [32] and OPAL [33, 34] experiments at CERN.

In the case of SIDIS observables, the experimental data correspond to the SIDIS cross section which is normalized to the inclusive DIS cross section. The SIDIS measurements have been reported both for the production of positive and negative charged hadrons. The COMPASS experiment at CERN [35, 36] and HERMES experiment at DESY [37] are two main experiments which have reported the experimental data for SIDIS processes for pion, kaon and unidentified light hadrons productions.

Considering the impact of nuclear PDF sets in SIDIS case, one should consider the nuclear PDF sets relevant to the nuclear target. COMPASS experiment has used a muon beam and a ^6LiD target. The data are collected by the HERMES experiment at the HERA storage ring using electron and positron beams on a hydrogen or deuterium gas target. Since `MontBlanc` unable to use different PDF sets at the same time to calculate the SIDIS observables,

we limit our study to the COMPASS data sets which reported 314 points for pion, kaon and unidentified light hadrons. The published HERMES data only include the 4 points and neglected in our study. The SIA and SIDIS experimental data for light charged hadron production used in our analysis follow those of our previous work [6]. We include all the charged pion and kaon data of SIA and SIDIS experiments, which are applied in recent analyses of MAPFF1.0 [5]. As we mentioned earlier the HERMES data is excluded from our analysis. More detailed study on the data selection can be found in Refs. [5, 6]. The proton PDF set of NNPDF3.0 has been used for determination of SIDIS observables as our baseline fit. Hence, in order to study the nuclear corrections one need to include the nuclear PDFs for ^6LiD .

All measured observables analyzed in this study along with their published references and the number of data points are presented in Tables. I and II for kaon, and in Tables. III and IV for the unidentified light charge hadrons, and in Tables. V and VI for pion. The values of individual and total χ^2 are presented for different PDF sets. In the case of SIA experimental data sets, the experimental data have reported as total inclusive, light-, charm-, and bottom-tagged cross sections measurements.

One needs to impose kinematical cuts on small and large values of z in which the perturbative fixed-order predictions should be reliable. We follow Refs. [5, 6] to apply the kinematic cuts on the SIA and SIDIS data sets. For the SIA data points, we apply the kinematic cuts on z based on the value of a center-of-mass (CM) energy: for data points with the scale of energy less than M_Z we use $0.075 \leq z \leq 0.9$, and for the data points with the scale of energy equal to M_Z we consider $0.02 \leq z \leq 0.9$.

For SIDIS, we consider the kinematical cut on the small Q and retain the experimental data points in region $Q \geq 2$ GeV. The same kinematical cuts are applied for charged pion, kaon and unidentified light hadrons analyses. In addition, since the small- z corrections at energy scale of B factories for kaon production occur at higher value of z in comparison with pion, we adopt $0.2 \leq z \leq 0.9$ for the BABAR experiments for kaon production.

IV. ANALYSIS SETUP AND FITTING PROCEDURE

After briefly presenting the flavor decomposition of FFs and related to observables of interest, we are in a position to discuss the analysis setup and fitting procedure.

We will state other theoretical choices and consider their effect on the extraction of FFs. The architecture of Neural Network used for parametrization is (1-20-7) which is quite simple but it proves to be sufficient [6] for the FFs analysis, it has 187 free parameters (weights and biases) need to be fixed from the data. To force the distributions to vanish at $z = 1$ and to be positive, value of NN at $z = 1$ (i.e. $\mathcal{N}(1; \theta)$) is subtracted from the output of the Neural Network and then the outcome is

squared, so the parametrization can be written as,

$$zD(z, \mu_0) = (\mathcal{N}(z; \boldsymbol{\theta}) - \mathcal{N}(1; \boldsymbol{\theta}))^2. \quad (4)$$

In the equation above, the \mathcal{N} represents a Neural Network with set of parameters $\boldsymbol{\theta}$, and the parametrization is assumed to be at $\mu_0 = 5$ GeV, above bottom quark mass threshold¹. This parametrization is used for both NLO and NNLO calculation with strong coupling constant $\alpha_S = 0.118$ at Z boson mass scale (91.1876 GeV) together with appropriate evolution.

As mentioned, the analysis made in this paper utilizes **MontBlanc** package, a C++ package dedicated to determination of collinear FFs [7]. In order to perform perturbative QCD analysis **MontBlanc** package uses the following packages; **GSL** or GNU scientific library for numerical utilities [38], **yaml-cpp** [39] for reading data and writing the results, **LHAPDF** library for reading input PDFs [40], **Ceres Solver** [41] for minimizing the χ^2 function, **NNAD** [42] for defining Neural Network and their derivatives, **APFEL++** [43] for evolution of FFs and **NangaParbat** [44] for calculation of observables. The χ^2 function minimized during analysis is defined as,

$$\chi_{(k)}^2 \equiv (\mathbf{T}(\boldsymbol{\theta}_{(k)}) - \mathbf{x}_{(k)})^T \cdot \mathbf{C}^{-1} \cdot (\mathbf{T}(\boldsymbol{\theta}_{(k)}) - \mathbf{x}_{(k)}), \quad (5)$$

where \mathbf{C}^{-1} is inverse of covariance matrix which includes all statistical and systematic uncertainties. The symbol $\mathbf{x}_{(k)}$ in represents k -th replica or pseudo-data set, analogously $\boldsymbol{\theta}_{(k)}$ is parameters of k -th Neural Network replica. Here \mathbf{T} represents the theoretical prediction calculated using mentioned Neural Network parameters. The symbol T indicates to the matrix transposing as usual. So far we have introduced the different parts of Eq. 5, now we are in a position to explain what we mean by replica. The method of Monte Carlo is used in this analysis to propagate experimental uncertainty to the resulting FFs. In this method a suitable ensemble of copies of data is chosen, after performing N_{rep} fits over individual (pseudo-)data sets in the ensemble, produced FFs are such that their simple statistical parameters as average and standard deviation constitute their central value and uncertainty, for more details see e.g. [6] and references therein.

To consider the SIDIS data, (nuclear)PDFs are needed to calculate the cross section. In **MontBlanc** approach a random replica of input PDF is chosen in every fit to incorporate PDF uncertainty in the determination of FFs. In spite of the fact that this source of uncertainty is shown to be a minor one [17], we opt for including it for the sake of completeness. Most of the available nuclear PDFs presented the uncertainty using the Hessian

method, and one need to convert the Hessian error sets into Monte Carlo using **MCGEN** code [45, 46] and then implement them in the analysis. The **MCGEN** creates Monte Carlo replicas using random displacement of Hessian sets and ensures that important properties of Hessian PDFs are preserved.

V. NUMERICAL RESULTS

In this section, we present the main results of this work and make a comparison between the calculated FFs with and without nuclear corrections. We first present the effect arising from nuclear corrections on our QCD analysis of kaon FFs. We discuss in details the effect on both the central values and on the error bands. Then we discuss the effect on the extracted unidentified charged hadron FFs and pion FFs as well. The impact arising from the nuclear corrections and higher-order QCD corrections on the individual and total χ^2 for different hadrons will be detailed.

A. Nuclear effects of the kaon FFs

In this section we mainly consider our results for the kaon FFs, in the presence of nuclear effects. As we discussed earlier, we consider the **NNPDF3.1** proton PDFs as our baseline fit. In order to investigate the impact arising from the inclusion of the nuclear effects at NLO accuracy, we consider three different sets of nuclear PDFs available in the literature, namely the **nNNPDF3.0** [12], **EPPS21** [13], and **nCTEQ15WZ** [14]. In order to examine the effect of nuclear corrections at a higher-order QCD correction, we use the **nNNPDF1.0** [15] in which provided the nuclear PDFs up to NNLO accuracy in perturbative QCD. The global QCD analyses reported by the **nNNPDF3.0**, **EPPS21**, and **nCTEQ15WZ** are limited to the NLO accuracy.

In the following, we present a short summary of these nuclear PDFs. The **nNNPDF3.0** [12] analysis presented an updated determination of nuclear PDF from a global datasets: the neutral-current (NC) nuclear fixed-target DIS measurements, the charged-current (CC) neutrino-nucleus DIS data, pPb collision at LHC for the boson production, data for CMS dijet [47], LHCb D0-meson production [48], isolated photon production [49] and fixed-target Drell-Yan (DY) measurements.

The **EPPS21** collaboration [13] has presented an updated nuclear PDF sets in **EPPS16** by new experimental data, the LHC pPb data for dijets (Run-I), D-mesons (Run-I) and W^\pm bosons (Run-II). In addition, they have included Jefferson Lab measurements of DIS which probe nuclear PDFs. In **EPPS21** the inclusive pion production at RHIC has been included and hence they have used a FF sets of pion in their analysis.

Recently, the **nCTEQ** Collaboration has extended the **nCTEQ15WZ** and included the W and Z data from pPb

¹ Mass thresholds considered to be, 1.51 GeV for charm and 4.92 GeV for bottom quark.

collisions at the LHC [14]. In addition to the nuclear DIS, DY lepton pair production, and RHIC pion data had been employed in the earlier nCTEQ15 analysis. They referred to it as nCTEQ15WZ and the accuracy is up to NLO.

We use the nNNPDF1.0 for calculation the FFs at NNLO [15]. The nNNPDF1.0 is the first determination of nuclear PDF based on the NNPDF methodology. The analysis is based on neutral-current structure functions on nuclear targets and is performed up to NNLO accuracy along with heavy quark mass effects.

In Table. I we show the individual value of χ^2/N_{dat} resulting from the FF fit at NLO accuracy considering NNPDF3.1 proton PDFs, and the nuclear PDF sets from nNNPDF3.0, EPPS21 and nCTEQ15WZ as well. The total value of $\chi^2/\text{d.o.f.}$ is shown at the bottom of this table. The value of χ^2/N_{dat} resulting from the FF fit at NNLO order by considering PDF sets of NNPDF3.1, and nuclear PDFs set from nNNPDF1.0 also shown in Table. II. The total value for $\chi^2/\text{d.o.f.}$ is shown as well. Considering the numbers presented in these tables for our kaon FFs, several comments are in order.

As one can see, the most interesting finding in our kaon FFs fit is the reduction of the total $\chi^2/\text{d.o.f.}$ after considering the nuclear PDFs. While the $\chi^2/\text{d.o.f.}$ for the NNPDF3.1 proton PDFs is 0.792, the inclusion of the nNNPDF3.0, EPPS21 and nCTEQ15WZ reduces the $\chi^2/\text{d.o.f.}$ to the 0.785, 0.749 and 0.704, respectively. The reduction of the individual χ^2 per data points are highlighted mostly for the case of COMPASS K^+ and COMPASS K^- data sets.

Another interesting finding is related to the inclusion of the higher-order QCD correction up to NNLO accuracy. As can be seen from Table. II, considering the NNLO accuracy in the case of proton PDF sets NNPDF3.1 could reduce the total $\chi^2/\text{d.o.f.}$ as expected. However, Table. II shows that the considering the nNNPDF1.0 NNLO nuclear PDFs could not improve the data/theory agreements. While the total $\chi^2/\text{d.o.f.}$ calculated using the NNPDF3.1 proton PDF is around 0.627, considering the nuclear correction increase it to the 0.731. More importantly, the individual χ^2 per data points for the COMPASS K^+ and COMPASS K^- data sets are increased to the 0.747 and 0.855 after the nuclear corrections are taken into account.

Now we are in a position to discuss the extracted kaon FFs, both in terms of central values and uncertainty bands, in the presence of nuclear effects and high-order QCD corrections. In Figs. 1 and 2, we present the kaon FFs for different parton species at NLO and NNLO accuracy. As we discussed earlier, the NNPDF3.1 proton PDFs is considered as our baseline, and the nuclear PDF sets from nNNPDF3.0, EPPS21 and nCTEQ15WZ are taken into account to examine the nuclear effects. We present both the absolute values, and the ratio to the NNPDF3.1 proton PDFs baseline as well. As one can see, including the nuclear PDFs changes both the shape of central values and uncertainties bands of extracted kaon FFs. Such

changes are more pronounced for the case of gluon, d and s FFs, at NLO accuracy. For the case of gluon and d FFs at NLO, the inclusion of nuclear effect not only affects the shape of central value, but also reduce uncertainty bands in respect to the NNPDF3.1 proton PDFs for most of regions of z .

For the case of \bar{s} , c^+ and b^+ the results are almost similar, however, reduction in the uncertainties can be seen for medium value of z for the \bar{s} , small value of z for the c^+ and large value of z for the b^+ after the inclusion of the nuclear PDFs. For the case of s and u , slight changes on both shape and uncertainties bands can be seen, and the inclusion of EPPS21 and nCTEQ15WZ decreases the bands slightly, however, the nNNPDF3.0 nuclear PDFs increase the error bands in most regions of z .

For almost all parton species, the smallest error bands are achieved using the nCTEQ15WZ nuclear PDFs in different region of z , which is more highlighted for the gluon, d , c^+ , s and u FFs.

The same findings as we discussed for the case of NLO, also hold for the NNLO results presented in Fig. 2. As can be seen, in terms of central values, the nuclear effects mostly affected the gluon, d and s FFs. The most noticeable changes for u and \bar{s} can be seen from medium to large z region. The behavior of central value of c^+ are almost the same with proton PDFs and nuclear PDFs in the whole region of z . The nuclear corrections also make change on b^+ FF at medium and large region of z . However, in terms of uncertainty bands, one can see that, the bands are reduced, and more importantly significant reduction for most of regions of z for gluon, d , s and u FFs and just for small values of z for \bar{s} and b^+ FFs can be observed. However, there is not any impressive changes at error bands for c^+ FFs after considering the nuclear corrections.

B. Nuclear effects of the unidentified light charged hadron FFs

Our results for the unidentified light charged hadron FFs, in the presence of nuclear effects, will be presented in this section. The individual and total χ^2 per data points for our charged hadron FFs analysis are presented in Table. III for NLO, and in Table. IV for NNLO accuracy. As can be seen, in terms of total χ^2 , the inclusion of the EPPS21 and nNNPDF3.0 nuclear PDFs reduce the values of χ^2 from 1.079 to 1.030 and 1.056, respectively. However, for the case of nCTEQ15WZ nuclear PDFs, almost the same χ^2 value is achieved in respect to NNPDF3.1 proton PDFs. This finding also consistent with the individual χ^2 per data points presented in Table. III, and more importantly for the COMPASS H^+ and COMPASS H^- data sets.

For the case of NNLO analysis, as can be seen from Table. IV, the inclusion of nuclear effects worsen the χ^2 numbers, both for the individual and total χ^2 per data points. This is mostly due to the increasing the value for individual χ^2 for both COMPASS H^+ and COMPASS H^-

Experiment	N_{dat}	$\frac{\chi^2}{N_{\text{dat}}}$ (NNPDF3.1)	$\frac{\chi^2}{N_{\text{dat}}}$ (nNNPDF3.0)	$\frac{\chi^2}{N_{\text{dat}}}$ (EPPS21)	$\frac{\chi^2}{N_{\text{dat}}}$ (nCTEQ15WZ)
COMPASS K^+ [35]	156	0.703	0.674	0.632	0.632
COMPASS K^- [35]	156	0.752	0.582	0.618	0.596
BELLE [28]	70	0.522	0.539	0.532	0.525
BABAR [26]	28	0.923	1.131	0.965	0.838
TASS012 [21]	3	0.785	0.779	0.785	0.791
TASS014 [22]	9	1.380	1.422	1.386	1.344
TASS022 [22]	6	0.672	0.636	0.665	0.712
TPC [25]	13	0.621	0.730	0.686	0.639
TASS034 [23]	5	0.038	0.035	0.037	0.041
TOPAZ [29]	3	0.127	0.147	0.146	0.143
ALEPH [30]	18	0.450	0.470	0.475	0.474
DELPHI (incl.) [32]	23	0.605	0.639	0.652	0.650
DELPHI (uds tag) [32]	23	0.280	0.260	0.276	0.293
DELPHI (b tag) [32]	23	0.696	0.918	0.770	0.610
OPAL (incl.) [33]	10	0.478	0.496	0.487	0.474
SLD (incl.) [27]	35	1.532	1.908	1.683	1.360
SLD (uds tag) [27]	35	1.751	1.877	1.784	1.674
SLD (b tag) [27]	35	2.339	2.768	2.429	2.043
Total $\chi^2/\text{d.o.f.}$	651	0.792	0.785	0.749	0.704

Table I: The list of input data sets for the kaon production included in our kaon FFs analysis. For each data set, we have indicated the experiments, corresponding published reference and the number of data points. In the last four columns, we show the value of χ^2/N_{dat} resulting from the FF fit at NLO order by considering the proton PDF sets from NNPDF3.1 and nuclear PDF sets available in the literature, namely the nNNPDF3.0 [12], EPPS21 [13], and nCTEQ15WZ [14]. The total value of $\chi^2/\text{d.o.f.}$ also is shown at the bottom of this table.

data sets.

Now we are in a position to discuss the extracted charged hadron FFs from our QCD analysis, determined from NNPDF3.1 proton PDFs and the available nuclear PDFs. The results are presented in Figs. 3 and 4, for the NLO and NNLO analysis. We present both the absolute values, and the ratio to the NNPDF3.1 proton PDFs baseline as well. For the case of unidentified charged hadron FFs, inclusion of nuclear effects mostly affected the central value of the gluon, d and \bar{d} FFs. Other FFs such as u and \bar{u} are slightly affected, especially over the medium to small value of z , c^+ and b^+ remain unchanged. As one can see, for the gluon, d and \bar{d} FFs, reduction of the error bands can be seen for medium to small value of z . The smaller error bands are correspond to the nCTEQ15WZ for the gluon FFs and the EPPS21 for the case of d and \bar{d} . The reduction of error bands for u and \bar{u} is very small in the some regions of z . In the case of c^+ the uncertainty bands almost do not change by considering the nuclear PDFs, although for b^+ FFs, one can see some differences for error bands at large value of z .

In Fig. 4, we present our results for the unidentified

light charged hadron FFs at NNLO accuracy considering the NNPDF3.1 proton PDFs, and nNNPDF1.0 nuclear PDFs. Like for the case of NLO analysis, for the c^+ FFs, both the central value and error bands remain unchanged after considering the nuclear corrections. While the corrections affect on the b^+ FFs from medium to large z region. All other FFs affected by the nuclear corrections, and reduction in uncertainty bands can be seen for the d , \bar{d} , u and \bar{u} for whole region of z . From Fig. 4, one can see that the gluon FFs behaves differently. Considering the nNNPDF1.0 nuclear PDFs the bands increase in respect to the NNPDF3.1 proton PDFs almost in all region of z . Although we can see the increasing of the χ^2 value in Table. IV after nuclear corrections, the uncertainty bands for most of the partons decrease due to the nuclear corrections.

Experiment	N_{dat}	$\frac{\chi^2}{N_{dat}}$ (NNPDF3.1)	$\frac{\chi^2}{N_{dat}}$ (nNNPDF1.0)
COMPASS K^+ [35]	156	0.616	0.747
COMPASS K^- [35]	156	0.620	0.855
BELLE [28]	70	0.478	0.489
BABAR [26]	28	0.373	0.426
TASS012 [21]	3	0.821	0.818
TASS014 [22]	9	1.261	1.257
TASS022 [22]	6	0.800	0.788
TPC [25]	13	0.519	0.485
TASS034 [23]	5	0.047	0.046
TOPAZ [29]	3	0.140	0.128
ALEPH [30]	18	0.454	0.500
DELPHI (incl.) [32]	23	0.774	0.745
DELPHI (uds tag) [32]	23	0.332	0.323
DELPHI (b tag) [32]	23	0.383	0.316
OPAL (incl.) [33]	10	0.386	0.437
SLD (incl.) [27]	35	0.705	0.709
SLD (uds tag) [27]	35	1.602	1.488
SLD (b tag) [27]	35	1.307	1.247
Total $\chi^2/\text{d.o.f.}$	651	0.627	0.731

Table II: Same as Table. I but this time for our kaon FFs at NNLO accuracy. The NNPDF3.1 proton PDFs are considered as our baseline fit, and the NNLO nuclear PDF set from nNNPDF1.0 also considered to study the nuclear corrections.

C. Nuclear effects of the pion FFs

In this section, we present the results for the pion FFs in the presence of nuclear corrections. The total and individual values for the χ^2 per data points are presented in Tables. V and VI for the NLO and NNLO analysis, respectively. For the case of our pion FFs analysis, the results and findings are different from those of kaon and unidentified charged hadron FFs analysis. As can be seen from Table. V, considering the nuclear PDFs from nNNPDF3.0, EPPS21 and nCTEQ15WZ do not improve the individual values for the χ^2 per data points. The total χ^2 value increases from 0.758 to 0.809, 1.456 and 0.761 for the different nuclear PDF sets. Even the χ^2 for the nCTEQ15WZ is very close to our baseline fit, but for the case of EPPS21 the fit leads to a large value. This is mostly due to the large χ^2 value for the COMPASS π^+ data sets. This finding also holds for the case of our NNLO analysis, in which considering the nNNPDF1.0 NNLO nuclear PDFs does not improve the fit. Again the χ^2 for the COMPASS π^+ is larger than those of our baseline fit. Another interesting find is related to the χ^2 values for the NLO and NNLO analysis. As one can see from Tables. V and VI, considering the higher-order QCD cor-

rection do not improve the fit quality for the pion FFs analysis. This finding also consistent with the study performed in Ref. [5] the inclusion of the NNLO corrections does not improve the fit quality.

In Fig. 5, we present the QCD fits in the presence of both the NNPDF3.1 proton PDFs as our baseline and three different sets of nuclear PDFs sets, at the NLO accuracy in perturbative QCD. In Fig. 6, the same comparisons are presented, but this time for the NNLO accuracy, and limited to the NNPDF3.1 proton PDFs and the nNNPDF1.0 nuclear PDFs. We present both the absolute values, and the ratio to the NNPDF3.1 proton PDFs baseline as well.

Considering the results presented in Figs. 5 and 6, several comments are in order. As one can see, including the nuclear PDFs, not only significantly change the shape of the central value of pion FFs, but also affect the error bands.

In term of individual flavor component of pion FFs at NLO accuracy, one can conclude the following: The biggest changes in the central values can be found for the case of gluon and \bar{d} FFs in the region $0.1 \leq z \leq 1$. One can see slight changes for s , u and d FFs in the whole region of z considering the nuclear corrections. In the case of c^+ and b^+ FFs the nuclear corrections affect only

Experiment	N_{dat}	$\frac{\chi^2}{N_{dat}}$ (NNPDF3.1)	$\frac{\chi^2}{N_{dat}}$ (nNNPDF3.0)	$\frac{\chi^2}{N_{dat}}$ (EPPS21)	$\frac{\chi^2}{N_{dat}}$ (nCTEQ15WZ)
COMPASS H^+ [36]	157	1.338	1.316	1.225	1.379
COMPASS H^- [36]	157	0.907	0.801	0.941	0.907
TASS014 [22]	14	1.791	1.820	1.805	1.734
TASS022 [22]	14	1.254	1.211	1.238	1.187
TPC [25]	21	0.659	0.605	0.613	0.508
TASS044 [23]	14	2.912	2.591	2.778	2.629
ALEPH [31]	32	0.825	0.822	0.830	0.817
DELPHI (incl.) [32]	21	0.610	0.602	0.594	0.592
DELPHI (uds tag) [32]	21	0.380	0.373	0.378	0.377
DELPHI (b tag) [32]	21	1.028	1.009	1.008	0.998
OPAL (incl.) [34]	19	1.821	1.824	1.774	1.785
OPAL (uds tag) [34]	19	0.794	0.788	0.798	0.787
OPAL (c tag) [34]	19	0.599	0.591	0.611	0.604
OPAL (b tag) [34]	19	0.299	0.278	0.287	0.281
SLD (incl.) [27]	34	1.047	1.044	1.086	1.086
SLD (uds tag) [27]	34	0.946	0.952	0.929	0.939
SLD (c tag) [27]	34	1.034	0.991	1.168	1.109
SLD (b tag) [27]	34	1.102	1.060	1.085	1.098
Total $\chi^2/\text{d.o.f.}$	684	1.079	1.030	1.056	1.080

Table III: The list of input data sets for our unidentified light charged hadrons production included in our charged hadron FFs analysis. For each data set, we have indicated the experiments, corresponding published reference and the number of data points. In the last four columns, we show the value of χ^2/N_{dat} resulting from the FF fit at NLO order by considering proton PDF sets from NNPDF3.1 and nuclear PDF sets available in the literature, namely nNNPDF3.0 [12], EPPS21 [13], and nCTEQ15WZ [14]. The total value of the total $\chi^2/\text{d.o.f.}$ also is shown at the bottom of the table.

the large z region. For all partons of pion FFs one can not find any improvement for error bands by applying these three nuclear PDF sets. The error uncertainties of inclusion of nCTEQ15WZ are smaller than nNNPDF3.0 and EPPS21 except in the small region of z . These results are consistent with the total χ^2 numbers reported in Table. V.

For the case of our NNLO pion results presented in Fig.6, the biggest changes can be seen for the gluon, \bar{d} , and u FFs. One can see minor changes in the central value of d , s , c^+ and b^+ by applying the nuclear PDF nNNPDF1.0. The improvements on the error bands upon inclusion of the nuclear effects can be found for the gluon, d , \bar{d} , and s FFs for the large value of z . For the case of u FFs, an improvement in the bands can be seen only for the small region of FFs. Overall speaking, nuclear corrections by utilizing the nNNPDF1.0 at NNLO accuracy could not reduce the uncertainties which and the number of total χ^2 after considering nuclear PDFs in Table. VI.

VI. SUMMARY AND CONCLUSIONS

In this work, we have presented the new global QCD analyses of FFs for pion, kaon and unidentified light charged hadrons, entitled as PKHFF.23, at NLO and NNLO accuracy in perturbative QCD. The experimental data from SIA and SIDIS processes are analyzed, and very recent studies presented in Refs. [5, 6] are revisited to examine the nuclear corrections on the SIDIS observables and on the newly extracted FFs. In this work, we have used Neural Network parametrization enriched with the Monte Carlo methodology for the uncertainty studies. This framework reduces the model bias as much as possible and the uncertainties of the experimental data and proton PDF sets properly propagate into the extracted FFs.

We have performed our QCD analyses which include NNPDF3.1 proton PDF set as baseline, and very recent determination of nuclear PDF sets available in literature namely the nNNPDF3.0, EPPS21, nCTEQ15WZ at NLO, and nNNPDF1.0 at NNLO to study the nuclear corrections.

Experiment	N_{dat}	$\frac{\chi^2}{N_{dat}}$ (NNPDF3.1)	$\frac{\chi^2}{N_{dat}}$ (nNNPDF1.0)
COMPASS H^+ [36]	157	1.711	2.340
COMPASS H^- [36]	157	1.301	2.455
TASS014 [22]	14	2.167	2.073
TASS022 [22]	14	1.241	1.218
TPC [25]	21	0.741	0.801
TASS044 [23]	14	2.466	2.491
ALEPH [31]	32	0.802	0.797
DELPHI (incl.) [32]	21	0.598	0.597
DELPHI (uds tag) [32]	21	0.374	0.407
DELPHI (b tag) [32]	21	1.030	1.068
OPAL (incl.) [34]	19	1.838	1.812
OPAL (uds tag) [34]	19	0.830	0.821
OPAL (c tag) [34]	19	0.603	0.610
OPAL (b tag) [34]	19	0.312	0.369
SLD (incl.) [27]	34	0.944	0.960
SLD (uds tag) [27]	34	0.941	0.922
SLD (c tag) [27]	34	1.115	1.156
SLD (b tag) [27]	34	1.225	1.330
Total $\chi^2/\text{d.o.f.}$	684	1.305	1.826

Table IV: Same as Table. III but this time for our unidentified light charged hadrons FFs at NNLO accuracy. The NNPDF3.1 proton PDFs are considered as out baseline fit, and the NNLO nuclear PDF set from nNNPDF1.0 also considered to study the nuclear corrections.

We show that utilizing the nuclear PDFs instead of proton PDF at NLO could reduce the individual χ^2 per data points of COMPASS and the total $\chi^2/\text{d.o.f.}$ value as well for charged kaon and unidentified light hadrons, and hence, could improve the fit quality. However, one can not see any improvement in the value of total $\chi^2/\text{d.o.f.}$ for the case of pion. In addition we have found that inclusion of the nuclear corrections changes both the shape of central values and uncertainties bands of extracted charged kaon, pion and unidentified light hadron for gluon and different quark species at NLO and NNLO accuracy.

In the case of kaon, for almost all parton species, the smaller error bands are achieved using the nCTEQ15WZ nuclear PDFs over different region of z at NLO accuracy. We have shown that the error bands for kaon are reduced at NNLO accuracy as well. In the case of unidentified light charged hadrons, by considering the nuclear corrections, for some of the partons, the error bands reduce, and for some others remained unchanged at both NLO and NNLO accuracy.

In the case of pion, the inclusion of nuclear corrections, specially the nCTEQ15WZ, improves the error bands at NLO accuracy. The improvements on the error bands

can be found for the large value of z at NNLO accuracy using the nNNPDF1.0 which is based only on the neutral-current nuclear DIS structure functions. However the reduction of the individual χ^2 of positive and negative COMPASS SIDIS data and the total $\chi^2/\text{d.o.f.}$ can not be seen clearly.

Overall speaking, in the case of NLO accuracy, the most promising results in terms of reduction of the values of individual χ^2 of positive and negative COMPASS SIDIS data, the total $\chi^2/\text{d.o.f.}$ and the error bands of various parton species are extracted considering the nCTEQ15WZ sets. In the case of NNLO accuracy, although the nuclear PDF sets of nNNPDF1.0 can not reduce the individual χ^2 of positive and negative COMPASS SIDIS data and the total $\chi^2/\text{d.o.f.}$, one can see the reduction of the uncertainty bands of extracted FFs.

ACKNOWLEDGMENTS

The authors gratefully acknowledge many helpful discussions and comments by Valerio Bertone. Authors thank the School of Particles and Accelerators, Institute

Experiment	N_{dat}	$\frac{\chi^2}{N_{dat}}$ (NNPDF3.1)	$\frac{\chi^2}{N_{dat}}$ (nNNPDF3.0)	$\frac{\chi^2}{N_{dat}}$ (EPPS21)	$\frac{\chi^2}{N_{dat}}$ (nCTEQ15WZ)
COMPASS π^+ [36]	157	0.601	0.731	3.176	0.593
COMPASS π^- [36]	157	0.417	0.422	0.471	0.430
BELLE[28]	70	0.093	0.092	0.095	0.093
BABAR [26]	39	1.286	1.300	1.284	1.375
TASS012 [21]	4	0.976	0.975	0.976	0.977
TASS014 [22]	9	1.376	1.389	1.380	1.374
TASS022 [22]	8	1.853	1.915	1.847	1.838
TPC [25]	13	0.223	0.229	0.226	0.223
TASS030 [21]	2	0.337	0.347	0.330	0.336
TASS034 [23]	9	1.190	1.353	1.189	1.165
TASS044 [23]	6	1.165	1.247	1.149	1.164
TOPAZ [29]	5	0.264	0.319	0.257	0.260
ALEPH [30]	23	1.121	1.139	0.990	1.164
DELPHI (incl.) [32]	21	1.312	1.311	1.407	1.305
DELPHI (uds tag) [32]	21	2.532	2.573	2.302	2.517
DELPHI (b tag) [32]	21	1.731	1.785	1.672	1.756
OPAL (incl.) [33]	24	1.629	1.674	1.561	1.661
SLD (incl.) [27]	34	1.102	1.096	0.950	1.087
SLD (uds tag) [27]	34	1.601	1.694	1.397	1.463
SLD (b tag) [27]	34	0.568	0.604	0.586	0.598
Total $\chi^2/\text{d.o.f.}$	691	0.758	0.809	1.456	0.761

Table V: The list of input data sets for the pion production included in our pion FFs analysis. For each data set, we have indicated the experiments, corresponding published reference and the number of data points. In the last four columns, we show the value of χ^2/N_{dat} resulting from the FF fit at NLO order by considering proton PDF sets from NNPDF3.1 and nuclear PDF sets available in the literature, nNNPDF3.0 [12], EPPS21 [13], and nCTEQ15WZ [14]. The total value of the total $\chi^2/\text{d.o.f.}$ also is shown at the bottom of the table.

for Research in Fundamental Sciences (IPM) for financial support of this project. Maryam Soleymaninia is thankful to the Iran Science Elites Federation for the financial support. Hamzeh Khanpour also is thankful to the Physics Department of University of Udine, and International Centre for Theoretical Physics (ICTP) for the financial support provided for this research.

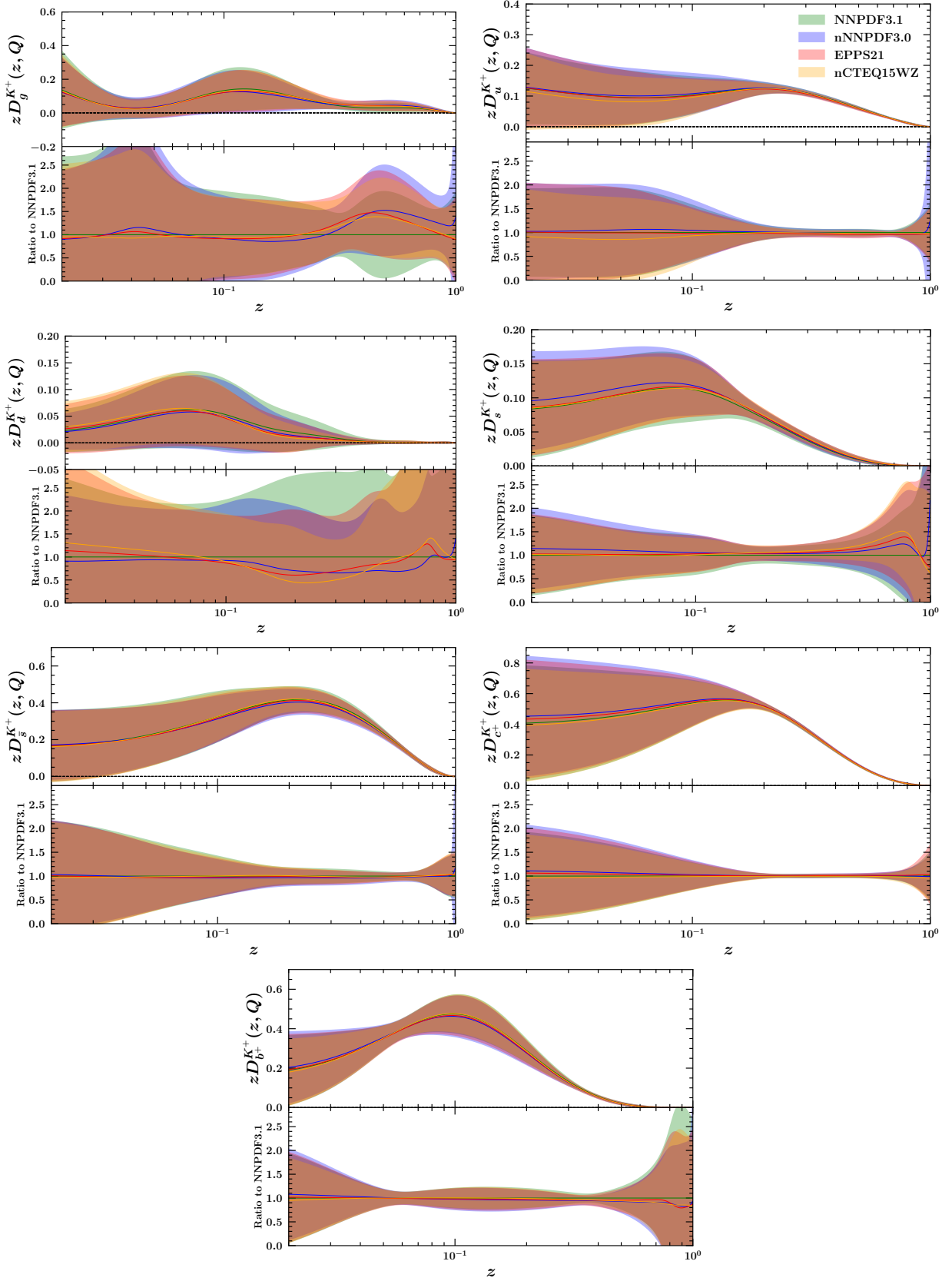


Figure 1: Comparison of kaon FFs extracted from NNPDF3.1 proton PDF sets as our baseline, and the nuclear PDF sets from nNNPDF3.0, EPPS21 and nCTEQ15WZ. We present both the absolute values, and the ratio to the NNPDF3.1 proton PDFs baseline as well. The results presented for the NLO accuracy at $Q = 5$ GeV.

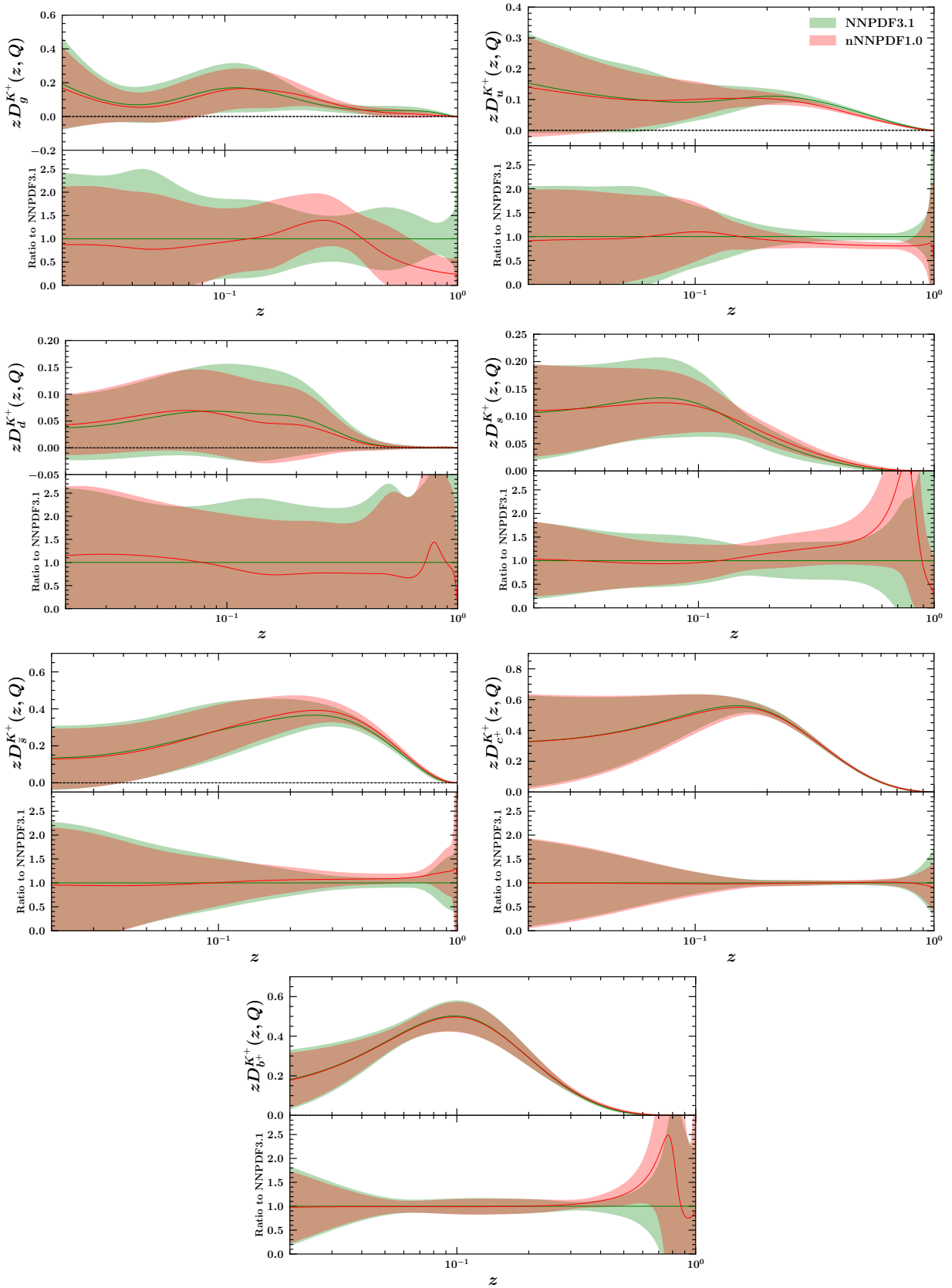


Figure 2: Same as Fig. 1 but this time for the NNLO accuracy. The NNPDF3.1 proton PDF sets are considered as our baseline fit, and the NNLO nuclear PDF sets from nNNPDF1.0 also considered to study the nuclear corrections.

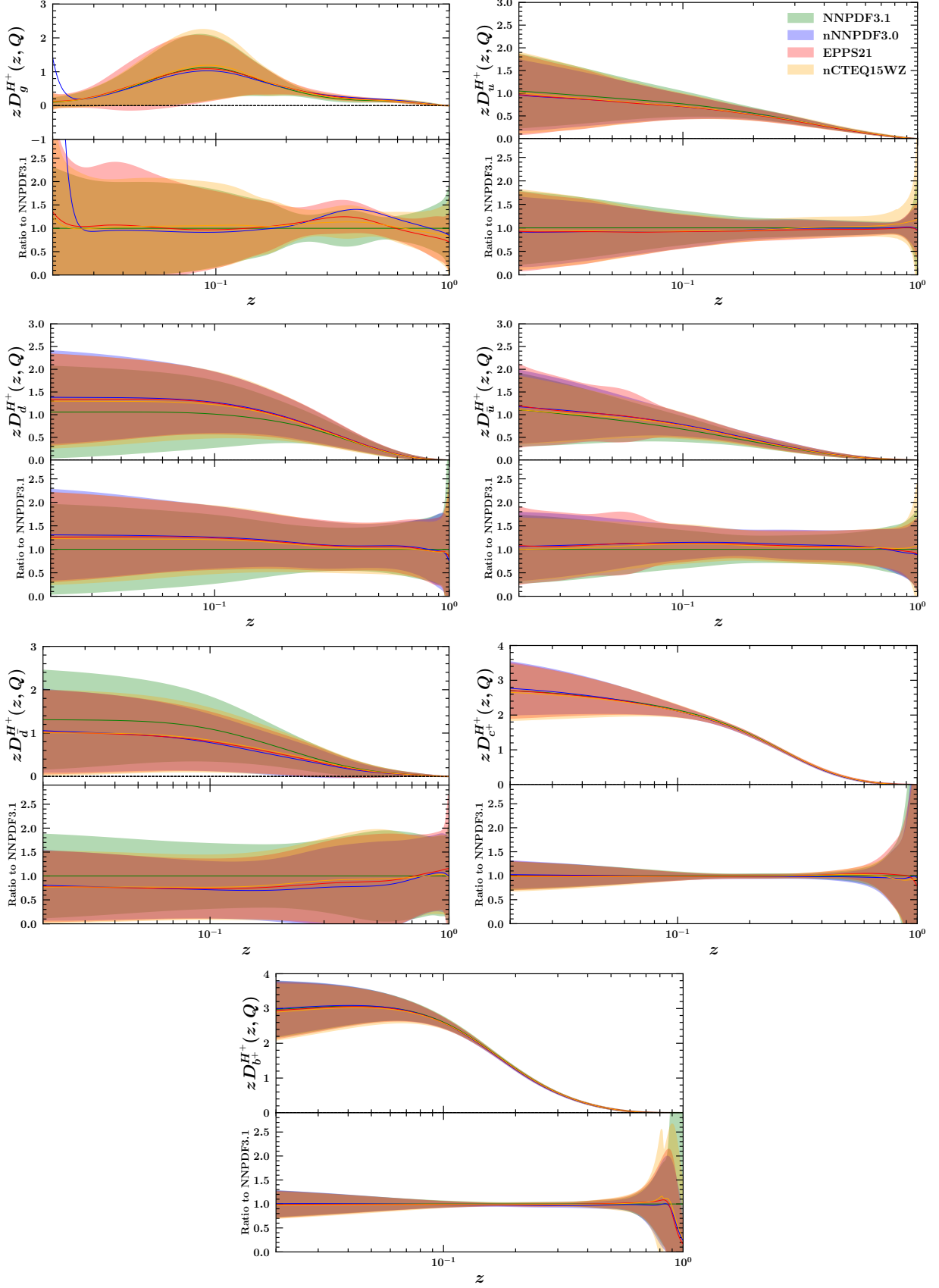


Figure 3: Comparison of charged hadron FFs extracted from NNPDF3.1 proton PDF sets as our baseline, and the nuclear PDF sets from nNNPDF3.0, EPPS21 and nCTEQ15WZ. We present both the absolute values, and the ratio to the NNPDF3.1 proton PDFs baseline as well. The results presented for the NLO accuracy at $Q = 5$ GeV.

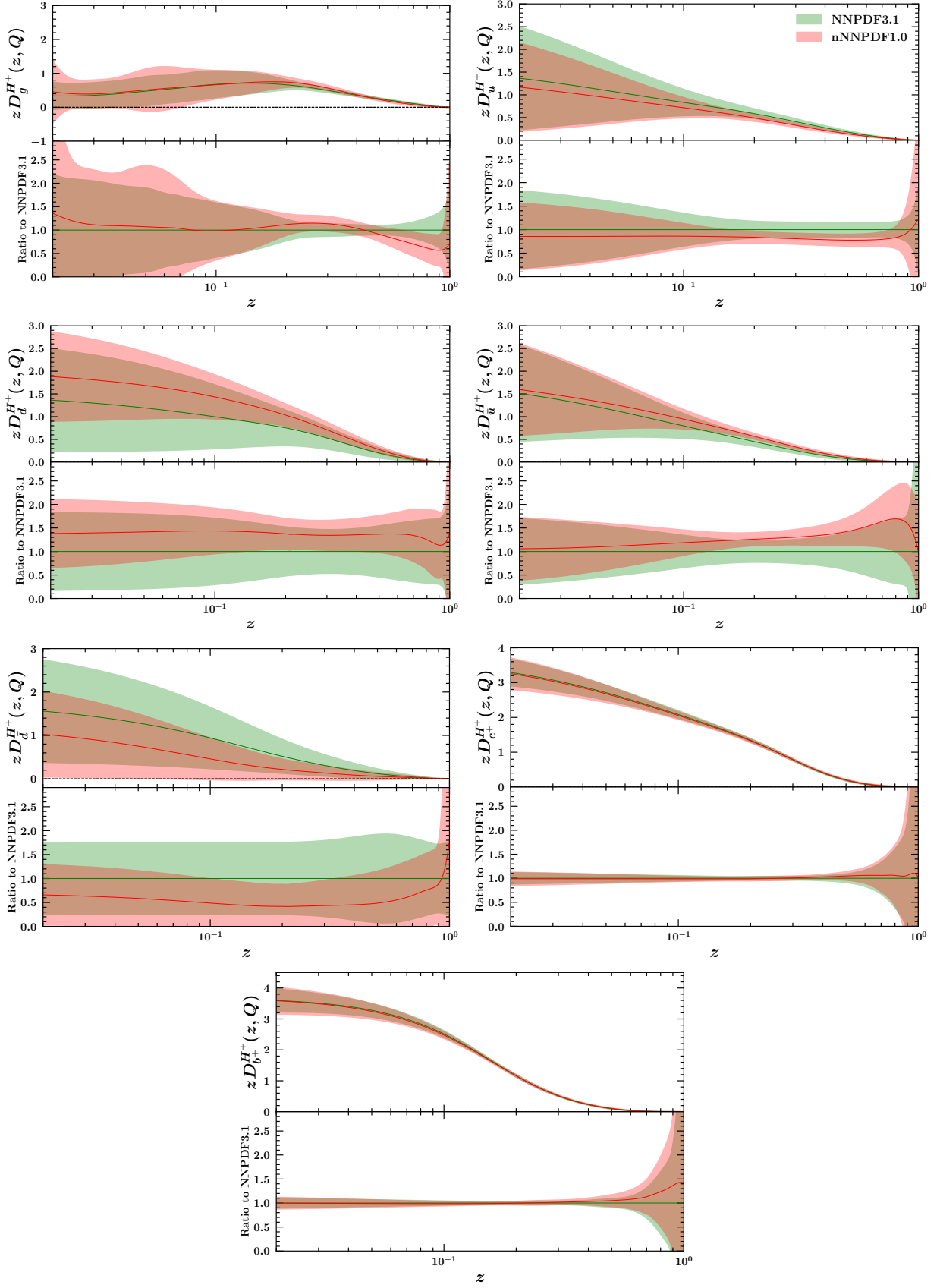


Figure 4: Same as Fig. 3 but this time for the NNLO accuracy. The NNPDF3.1 proton PDF sets are considered as our baseline fit, and the NNLO nuclear PDF sets from nNNPDF1.0 also considered to study the nuclear corrections.

Experiment	N_{dat}	$\frac{\chi^2}{N_{dat}}$ (NNPDF3.1)	$\frac{\chi^2}{N_{dat}}$ (nNNPDF1.0)
COMPASS π^+ [36]	157	0.989	1.208
COMPASS π^- [36]	157	0.564	0.640
BELLE [28]	70	0.096	0.095
BABAR [26]	39	1.012	1.073
TASS012 [21]	4	0.972	0.973
TASS014 [22]	9	1.387	1.386
TASS022 [22]	8	1.931	1.900
TPC [25]	13	0.265	0.267
TASS030 [21]	2	0.354	0.352
TASS034 [23]	9	1.494	1.431
TASS044 [23]	6	1.360	1.364
TOPAZ [29]	5	0.360	0.355
ALEPH [30]	23	1.306	1.228
DELPHI (incl.) [32]	21	1.281	1.295
DELPHI (uds tag) [32]	21	2.745	2.669
DELPHI (b tag) [32]	21	1.812	1.824
OPAL (incl.) [33]	24	1.739	1.733
SLD (incl.) [27]	34	1.039	1.008
SLD (uds tag) [27]	34	1.968	1.870
SLD (b tag) [27]	34	0.678	0.651
Total $\chi^2/\text{d.o.f.}$	691	0.935	1.008

Table VI: Same as Table. V but this time for our pion FFs at NNLO accuracy. The NNPDF3.1 proton PDFs are considered as our baseline fit, and the NNLO nuclear PDF set from nNNPDF1.0 also considered to study the nuclear corrections.

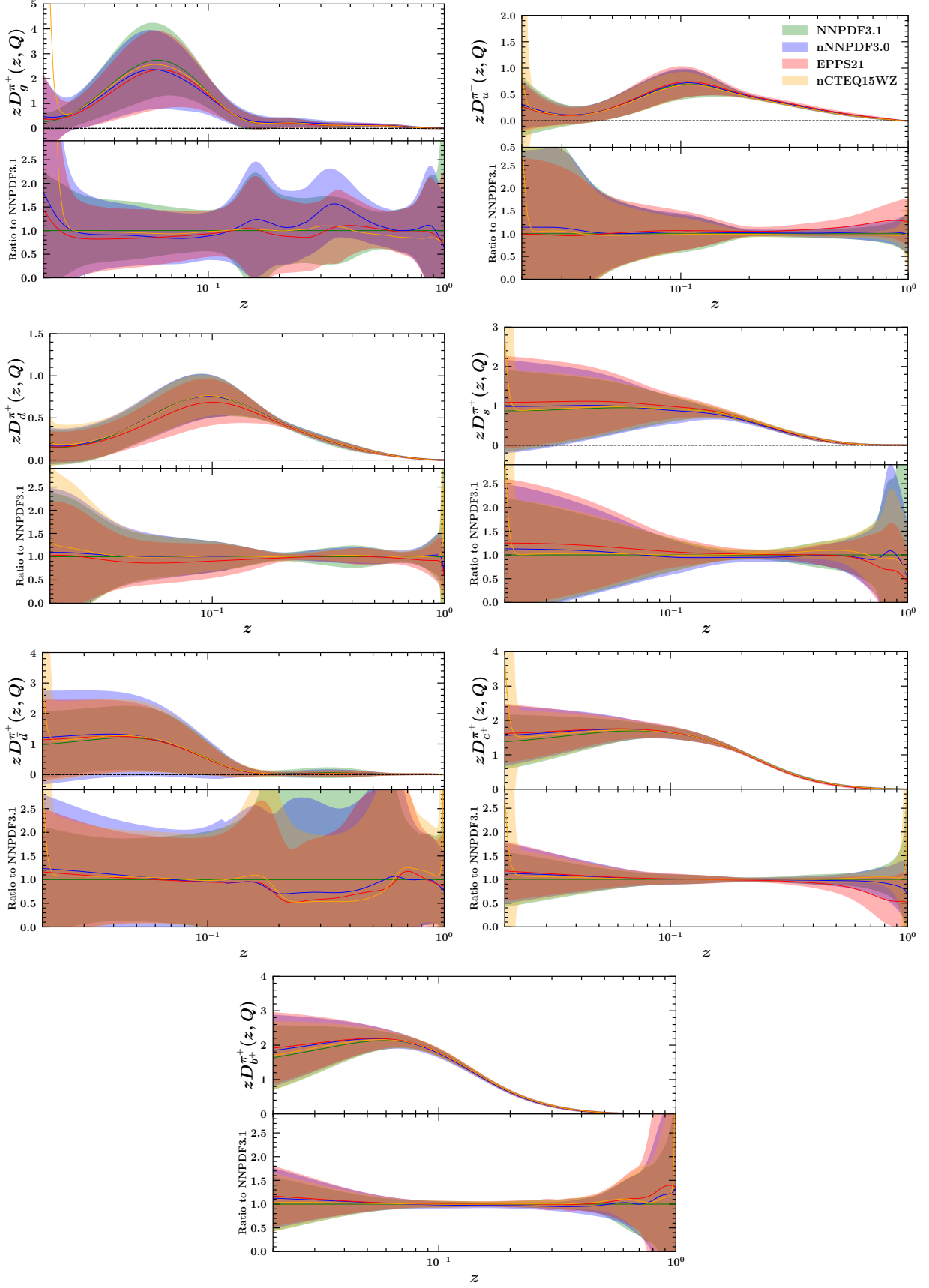


Figure 5: Comparison of pion FFs extracted from NNPDF3.1 proton PDF sets as our baseline, and the nuclear PDF sets from nNNPDF3.0, EPPS21 and nCTEQ15WZ. We present both the absolute values, and the ratio to the NNPDF3.1 proton PDFs baseline as well. The results presented for the NLO accuracy at $Q = 5$ GeV.

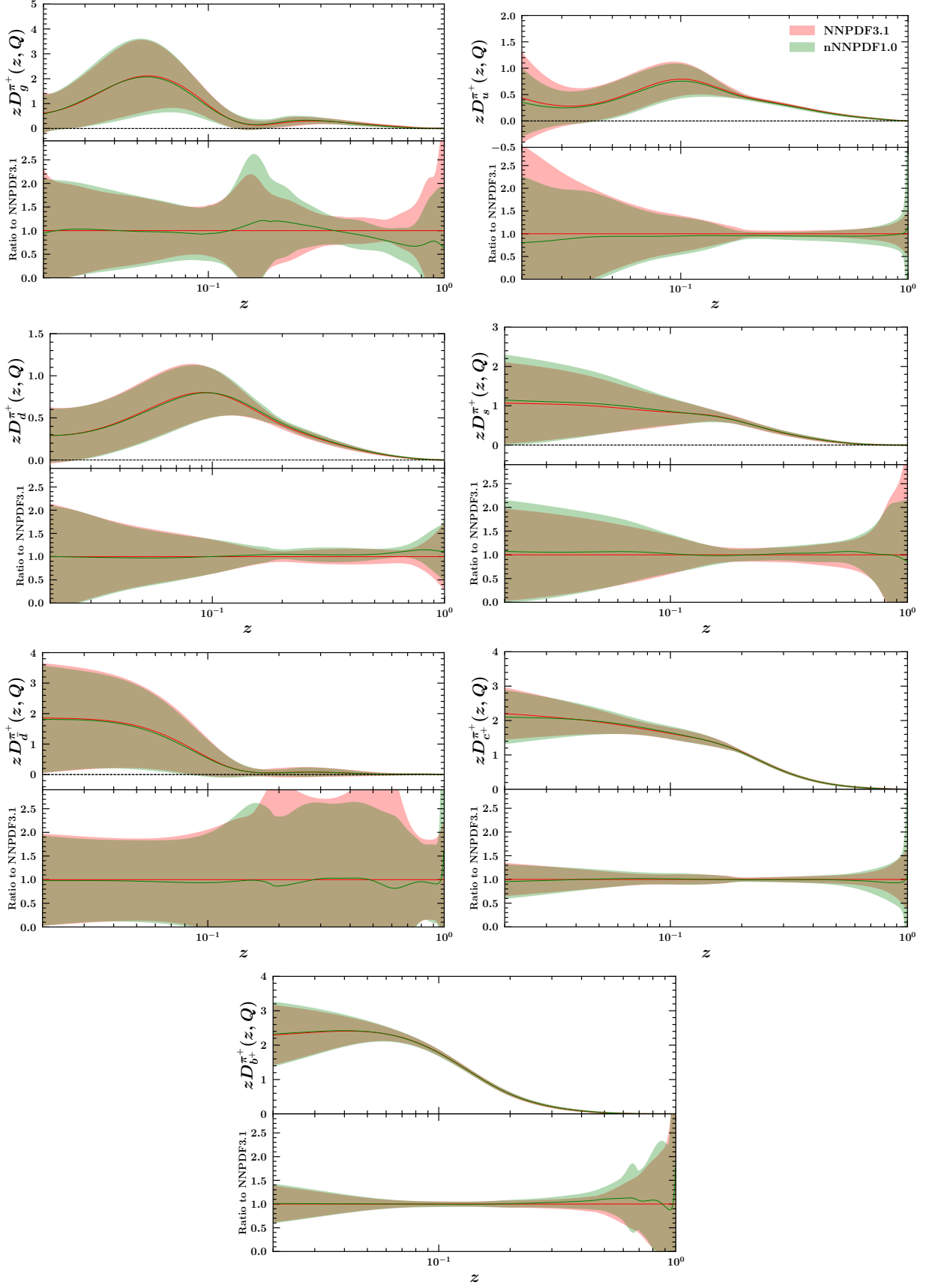


Figure 6: Same as Fig. 5 but this time for the NNLO accuracy. The NNPDF3.1 proton PDF sets are considered as our baseline fit, and the NNLO nuclear PDF sets from nNNPDF1.0 also considered to study the nuclear corrections.

-
- [1] A. C. Aguilar, Z. Ahmed, C. Aidala, S. Ali, V. Andrieux, J. Arrington, A. Bashir, V. Berdnikov, D. Binosi and L. Chang, *et al.* “Pion and Kaon Structure at the Electron-Ion Collider,” *Eur. Phys. J. A* **55**, no.10, 190 (2019) doi:10.1140/epja/i2019-12885-0 [arXiv:1907.08218 [nucl-ex]].
- [2] R. Abdul Khalek, A. Accardi, J. Adam, D. Adamiak, W. Akers, M. Albaladejo, A. Al-bataineh, M. G. Alexeev, F. Ameli and P. Antonioli, *et al.* “Science Requirements and Detector Concepts for the Electron-Ion Collider: EIC Yellow Report,” *Nucl. Phys. A* **1026**, 122447 (2022) doi:10.1016/j.nuclphysa.2022.122447 [arXiv:2103.05419 [physics.ins-det]].
- [3] A. Abada *et al.* [FCC], “FCC Physics Opportunities: Future Circular Collider Conceptual Design Report Volume 1,” *Eur. Phys. J. C* **79**, no.6, 474 (2019) doi:10.1140/epjc/s10052-019-6904-3
- [4] A. Abada *et al.* [FCC], “FCC-hh: The Hadron Collider: Future Circular Collider Conceptual Design Report Volume 3,” *Eur. Phys. J. ST* **228**, no.4, 755-1107 (2019) doi:10.1140/epjst/e2019-900087-0
- [5] R. Abdul Khalek, V. Bertone, A. Khoukli and E. R. Nocera, “Pion and kaon fragmentation functions at next-to-next-to-leading order,” *Phys. Lett. B* **834**, 137456 (2022) doi:10.1016/j.physletb.2022.137456 [arXiv:2204.10331 [hep-ph]].
- [6] M. Soleymaninia, H. Hashamipour and H. Khanpour, “Neural network QCD analysis of charged hadron fragmentation functions in the presence of SIDIS data,” *Phys. Rev. D* **105**, no.11, 11 (2022) doi:10.1103/PhysRevD.105.114018 [arXiv:2202.10779 [hep-ph]].
- [7] <https://github.com/MapCollaboration/MontBlanc>
- [8] P. J. Rijken and W. L. van Neerven, “Higher order QCD corrections to the transverse and longitudinal fragmentation functions in electron - positron annihilation,” *Nucl. Phys. B* **487**, 233-282 (1997) doi:10.1016/S0550-3213(96)00669-4 [arXiv:hep-ph/9609377 [hep-ph]].
- [9] A. A. Almasy, S. Moch and A. Vogt, “On the Next-to-Next-to-Leading Order Evolution of Flavour-Singlet Fragmentation Functions,” *Nucl. Phys. B* **854**, 133-152 (2012) doi:10.1016/j.nuclphysb.2011.08.028 [arXiv:1107.2263 [hep-ph]].
- [10] M. Abele, D. de Florian and W. Vogelsang, “Approximate NNLO QCD corrections to semi-inclusive DIS,” *Phys. Rev. D* **104**, no.9, 094046 (2021) doi:10.1103/PhysRevD.104.094046 [arXiv:2109.00847 [hep-ph]].
- [11] R. D. Ball *et al.* [NNPDF], “Parton distributions from high-precision collider data,” *Eur. Phys. J. C* **77**, no.10, 663 (2017).
- [12] R. Abdul Khalek, R. Gauld, T. Giani, E. R. Nocera, T. R. Rabemananjara and J. Rojo, “nNNPDF3.0: evidence for a modified partonic structure in heavy nuclei,” *Eur. Phys. J. C* **82**, no.6, 507 (2022) doi:10.1140/epjc/s10052-022-10417-7 [arXiv:2201.12363 [hep-ph]].
- [13] K. J. Eskola, P. Paakkinen, H. Paukkunen and C. A. Salgado, “EPPS21: a global QCD analysis of nuclear PDFs,” *Eur. Phys. J. C* **82**, no.5, 413 (2022) doi:10.1140/epjc/s10052-022-10359-0 [arXiv:2112.12462 [hep-ph]].
- [14] A. Kusina, T. Ježo, D. B. Clark, P. Duwentäster, E. Godat, T. J. Hobbs, J. Kent, M. Klasen, K. Kovařík and F. Lyonnet, *et al.* “Impact of LHC vector boson production in heavy ion collisions on strange PDFs,” *Eur. Phys. J. C* **80**, no.10, 968 (2020) doi:10.1140/epjc/s10052-020-08532-4 [arXiv:2007.09100 [hep-ph]].
- [15] R. Abdul Khalek *et al.* [NNPDF], “Nuclear parton distributions from lepton-nucleus scattering and the impact of an electron-ion collider,” *Eur. Phys. J. C* **79**, no.6, 471 (2019) doi:10.1140/epjc/s10052-019-6983-1 [arXiv:1904.00018 [hep-ph]].
- [16] R. K. Ellis, W. J. Stirling, and B. R. Webber, *QCD and Collider Physics*, Cambridge University Press (1996).
- [17] R. A. Khalek, V. Bertone and E. R. Nocera, “Determination of unpolarized pion fragmentation functions using semi-inclusive deep-inelastic-scattering data,” *Phys. Rev. D* **104**, no.3, 034007 (2021) doi:10.1103/PhysRevD.104.034007 [arXiv:2105.08725 [hep-ph]].
- [18] E. Moffat *et al.* [Jefferson Lab Angular Momentum (JAM)], “Simultaneous Monte Carlo analysis of parton densities and fragmentation functions,” *Phys. Rev. D* **104**, no.1, 016015 (2021).
- [19] H. Abdolmaleki *et al.* [xFitter Developers’ Team], “QCD analysis of pion fragmentation functions in the xFitter framework,” *Phys. Rev. D* **104**, no.5, 056019 (2021).
- [20] V. Bertone *et al.* [NNPDF], “A determination of the fragmentation functions of pions, kaons, and protons with faithful uncertainties,” *Eur. Phys. J. C* **77**, no.8, 516 (2017).
- [21] R. Brandelik *et al.* [TASSO], “Charged Pion, Kaon, Proton and anti-Proton Production in High-Energy e^+e^- Annihilation,” *Phys. Lett. B* **94**, 444-449 (1980) doi:10.1016/0370-2693(80)90915-6.
- [22] M. Althoff *et al.* [TASSO], “Charged Hadron Composition of the Final State in e^+e^- Annihilation at High-Energies,” *Z. Phys. C* **17**, 5-15 (1983) doi:10.1007/BF01577813.
- [23] W. Braunschweig *et al.* [TASSO], “Pion, Kaon and Proton Cross-sections in e^+e^- Annihilation at 34-GeV and 44-GeV Center-of-mass Energy,” *Z. Phys. C* **42**, 189 (1989) doi:10.1007/BF01555856.
- [24] W. Braunschweig *et al.* [TASSO], “Global Jet Properties at 14-GeV to 44-GeV Center-of-mass Energy in e^+e^- Annihilation,” *Z. Phys. C* **47**, 187-198 (1990) doi:10.1007/BF01552339.
- [25] H. Aihara *et al.* [TPC/Two Gamma Collaboration], “Charged hadron inclusive cross-sections and fractions in e^+e^- annihilation $\sqrt{s} = 29$ GeV,” *Phys. Rev. Lett.* **61**, 1263 (1988).
- [26] J. P. Lees *et al.* [BaBar], “Production of charged pions, kaons, and protons in e^+e^- annihilations into hadrons at $\sqrt{s}=10.54$ GeV,” *Phys. Rev. D* **88**, 032011 (2013).
- [27] K. Abe *et al.* [SLD Collaboration], “Production of π^+ , π^- , K^+ , K^- , p and anti- p in light (uds), c and b jets from Z^0 decays,” *Phys. Rev. D* **69**, 072003 (2004).
- [28] M. Leitgab *et al.* [Belle], “Precision Measurement of Charged Pion and Kaon Differential Cross Sections in e^+e^- Annihilation at $s=10.52$ GeV,” *Phys. Rev. Lett.* **111**, 062002 (2013) doi:10.1103/PhysRevLett.111.062002

- [arXiv:1301.6183 [hep-ex]].
- [29] R. Itoh *et al.* [TOPAZ], “Measurement of inclusive particle spectra and test of MLLA prediction in e^+e^- annihilation at $s^{*1/2} = 58\text{-GeV}$,” *Phys. Lett. B* **345**, 335-342 (1995) doi:10.1016/0370-2693(94)01685-6 [arXiv:hep-ex/9412015 [hep-ex]].
- [30] D. Buskulic *et al.* [ALEPH], “Inclusive π^+ , K^+ and $(p, \text{anti-}p)$ differential cross-sections at the Z resonance,” *Z. Phys. C* **66**, 355-366 (1995) doi:10.1007/BF01556360.
- [31] D. Buskulic *et al.* [ALEPH Collaboration], “Measurement of α_s from scaling violations in fragmentation functions in e^+e^- annihilation,” *Phys. Lett. B* **357**, 487 (1995), Erratum: *Phys. Lett. B* **364**, 247 (1995).
- [32] P. Abreu *et al.* [DELPHI Collaboration], “ π^\pm , K^\pm , p and \bar{p} production in $Z^0 \rightarrow q\bar{q}$, $Z^0 \rightarrow b\bar{b}$, $Z^0 \rightarrow u\bar{u}, d\bar{d}, s\bar{s}$,” *Eur. Phys. J. C* **5**, 585 (1998).
- [33] R. Akers *et al.* [OPAL], “Measurement of the production rates of charged hadrons in e^+e^- annihilation at the Z0,” *Z. Phys. C* **63**, 181-196 (1994) doi:10.1007/BF01411010.
- [34] K. Ackerstaff *et al.* [OPAL Collaboration], “Measurements of flavor dependent fragmentation functions in $Z^0 \rightarrow q \text{ anti-}q$ events,” *Eur. Phys. J. C* **7**, 369 (1999).
- [35] C. Adolph *et al.* [COMPASS], “Multiplicities of charged kaons from deep-inelastic muon scattering off an isoscalar target,” *Phys. Lett. B* **767**, 133-141 (2017) doi:10.1016/j.physletb.2017.01.053 [arXiv:1608.06760 [hep-ex]].
- [36] C. Adolph *et al.* [COMPASS], “Multiplicities of charged pions and charged hadrons from deep-inelastic scattering of muons off an isoscalar target,” *Phys. Lett. B* **764**, 1-10 (2017).
- [37] A. Airapetian *et al.* [HERMES], “Multiplicities of charged pions and kaons from semi-inclusive deep-inelastic scattering by the proton and the deuteron,” *Phys. Rev. D* **87**, 074029 (2013).
- [38] <https://www.gnu.org/software/gsl>
- [39] <https://github.com/jbeder/yaml-cpp>
- [40] A. Buckley, J. Ferrando, S. Lloyd, K. Nordström, B. Page, M. Rüfenacht, M. Schönherr and G. Watt, “LHAPDF6: parton density access in the LHC precision era,” *Eur. Phys. J. C* **75**, 132 (2015).
- [41] S. Agarwal, K. Mierle, and Others, “Ceres solver.” <http://ceres-solver.org>.
- [42] <https://github.com/rabah-khalek/NNAD>
- [43] V. Bertone, “APFEL++: A new PDF evolution library in C++,” *PoS DIS2017*, 201 (2018).
- [44] <https://github.com/MapCollaboration/NangaParbat>
- [45] T. J. Hou, J. Gao, J. Huston, P. Nadolsky, C. Schmidt, D. Stump, B. T. Wang, K. P. Xie, S. Dulat and J. Pumplin, *et al.* “Reconstruction of Monte Carlo replicas from Hessian parton distributions,” *JHEP* **03**, 099 (2017).
- [46] V. Bertone, private communication.
- [47] A. M. Sirunyan *et al.* [CMS], “Constraining gluon distributions in nuclei using dijets in proton-proton and proton-lead collisions at $\sqrt{s_{NN}} = 5.02\text{ TeV}$,” *Phys. Rev. Lett.* **121**, no.6, 062002 (2018) doi:10.1103/PhysRevLett.121.062002 [arXiv:1805.04736 [hep-ex]].
- [48] R. Aaij *et al.* [LHCb], “Study of prompt D^0 meson production in $p\text{Pb}$ collisions at $\sqrt{s_{NN}} = 5\text{ TeV}$,” *JHEP* **10**, 090 (2017) doi:10.1007/JHEP10(2017)090 [arXiv:1707.02750 [hep-ex]].
- [49] M. Aaboud *et al.* [ATLAS], “Measurement of prompt photon production in $\sqrt{s_{NN}} = 8.16\text{ TeV } p\text{+Pb}$ collisions with ATLAS,” *Phys. Lett. B* **796**, 230-252 (2019) doi:10.1016/j.physletb.2019.07.031 [arXiv:1903.02209 [nucl-ex]].